JACS
JOURNAL OF THE AMERICAN CHEMICAL SOCIETY

Article

pubs.acs.org/JACS

Multifunctional Tumor pH-Sensitive Self-Assembled Nanoparticles for Bimodal Imaging and Treatment of Resistant Heterogeneous Tumors

Daishun Ling,[†,‡,#] Wooram Park,[§,#] Sin-jung Park,[§] Yang Lu,[†,‡] Kyoung Sub Kim,[§] Michael J. Hackett,[†,‡] Byung Hyo Kim,[†,‡] Hyeona Yim,[§] Yong Sun Jeon,[∥] Kun Na,*[,§] and Taeghwan Hyeon*[,†,‡]

[†]Center for Nanoparticle Research, Institute for Basic Science (IBS), Seoul 151-742, Korea

[‡]School of Chemical and Biological Engineering, Seoul National University, Seoul 151-742, Korea

[§]Department of Biotechnology, The Catholic University of Korea, Bucheon-si, Gyeonggi-do 420-743, Korea

[∥]Department of Radiology, Inha University College of Medicine, Incheon 420-751, Korea

Supporting Information

ABSTRACT: Nanoparticle-based diagnosis−therapy integrative systems represent an emerging approach to cancer treatment. However, the diagnostic sensitivity, treatment efficacy, and bioavailability of nanoparticles as well as the heterogeneity and drug resistance of tumors pose tremendous challenges for clinical implementation. We herein report on the fabrication of tumor pH-sensitive magnetic nanogrenades (termed PMNs) composed of self-assembled iron oxide nanoparticles and pH-responsive ligands. These PMNs can readily target tumors via surface-charge switching triggered by the acidic tumor microenvironment, and are further disassembled into a highly active state in acidic subcellular compartments that "turns on" MR contrast, fluorescence and photodynamic therapeutic activity. We successfully visualized small tumors implanted in mice via unique pH-responsive T_1MR contrast and fluorescence, demonstrating early stage diagnosis of tumors without using any targeting agents. Furthermore, pH-triggered generation of singlet oxygen enabled pH-dependent photodynamic therapy to selectively kill cancer cells. In particular, we demonstrated the superior therapeutic efficacy of PMNs in highly heterogeneous drug-resistant tumors, showing a great potential for clinical applications.

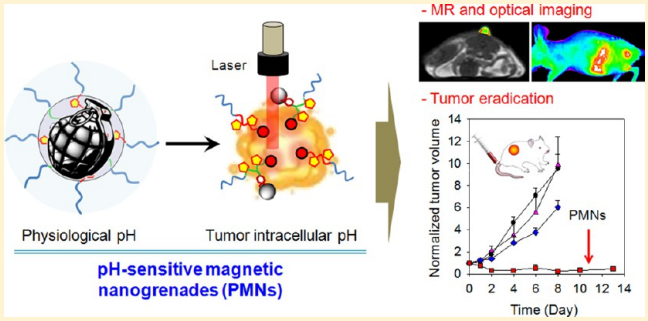

INTRODUCTION

Tumors in patients generally contain heterogeneous cell populations,[1,2] and tumor heterogeneity greatly influences the effectiveness of the receptor−ligand targeting strategies that are most popularly used in cancer nanotechnology.[3] Furthermore, the heterogeneous tumoral extracellular matrix impedes drug penetration which reduces drug exposure and gradually induces drug-resistance.[4] The tumor microenvironment exhibits an increased interstitial fluid pressure caused by leaky vasculature, poor lymphatic drainage, and a high density of cells and associated matrices.[5] Consequently, the penetration of nanoparticle-based drugs is limited to the tumor peripheral region with little diffusion of therapeutic nanoparticles into the tumor interstitial space.[5] The physiological and physical mechanism of drug resistance as a whole is a major cause of the failure of most cancer treatments. Although nanoparticles of small size and multifunctionality[6−11] are emerging as the next-generation anticancer agents,[12−19] there remain great challenges to the development of 'smart' nanoparticles that can specifically respond to tumor-associated stimuli in order to overcome the aforementioned tumoral barriers.

Self-assembly provides a simple, reproducible, and inexpensive way of generating ensembles of nanoparticles[20] with unique plasmonic,[21−23] photoluminescent,[24] and magnetic properties[25] in a controllable manner. Several stimulus-responsive assembled nanostructures have been thoroughly examined as bio- or chemo-sensors *in vitro*.[26−30] However, thus far, these types of "smart" ensembles have rarely been investigated *in vivo* owing primarily to these inherent physiological obstacles. One commonality among tumors is acidity; the microenvironment usually has a pH of ∼6.8[5,31] and endo/lysosomes experience even lower pH values of 5.0−5.5.[32] Demonstrated here is a self-assembly of iron oxide nanoparticles assisted by engineered polymeric ligands, termed pH-sensitive magnetic nanogrenades (PMNs) that activate under these tumor pH conditions for ultrasensitive bimodal imaging and treatment of resistant heterogeneous tumors *in vivo* (Scheme 1).

Received: October 22, 2013
Published: April 1, 2014

   dx.doi.org/10.1021/ja4108287 | *J. Am. Chem. Soc.* 2014, 136, 5647−5655

Scheme 1. Design and Mechanism of pH-Sensitive Magnetic Nanogrenades (PMNs) for Tumor pH Activation; (a) Schematic Representation of pH-Responsive, Ligand-Assisted Self-Assembly of Extremely Small Iron Oxide Nanoparticles (ESIONs); (b.c) Schematic Representation of Tumor pH-Recognizable Treatment Strategy Using PMNs[a]

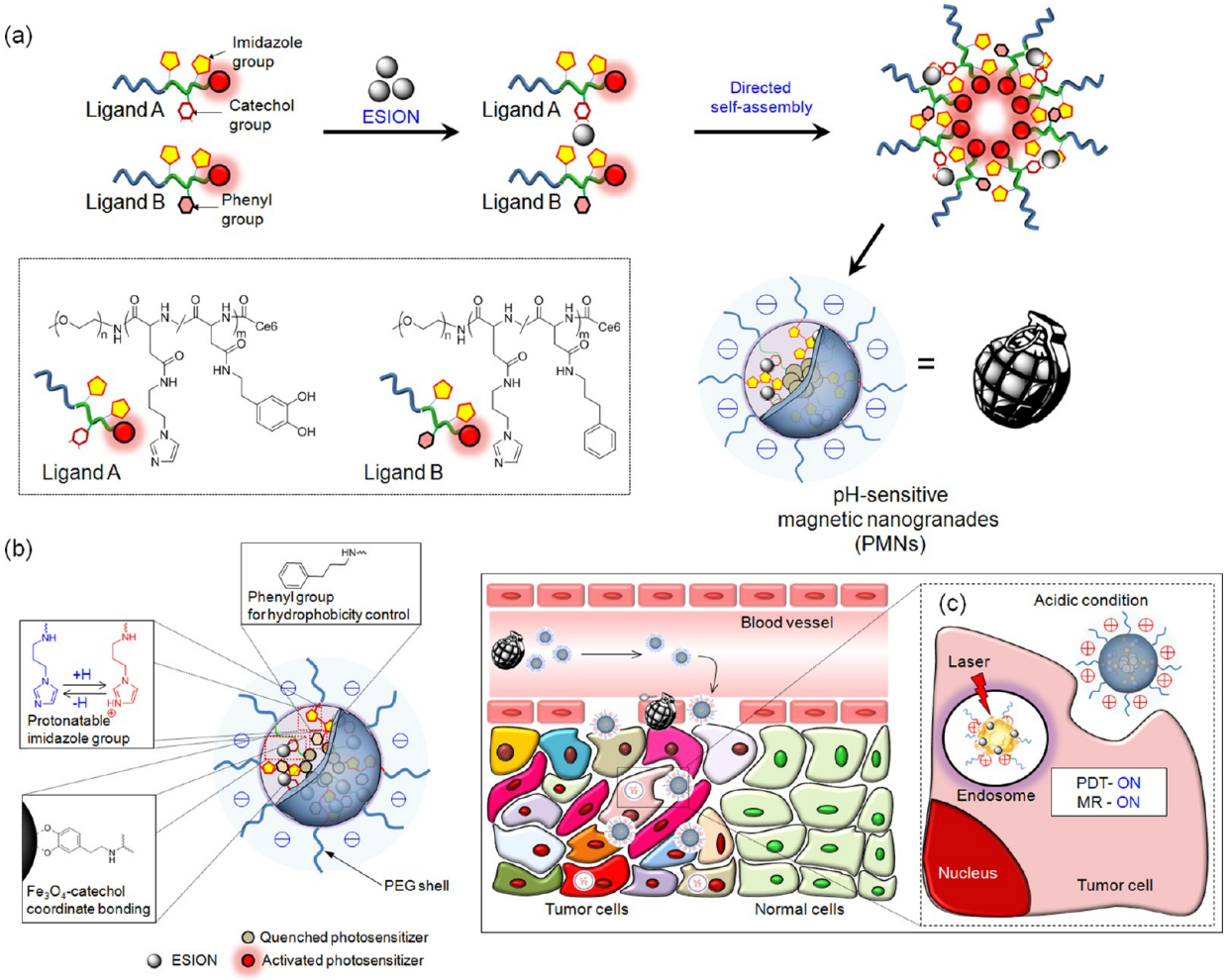

[a]PMNs are latent in the circulation and reverse their surface charge from negative to positive at the tumor extracellular pH (~6.8) to facilitate tissue permeation in the tumor microenvironment, trigger cell internalization where the decreased pH (~5.5) causes further disassembly to enhanced their MR contrast and photoactivity.

EXPERIMENTAL SECTION

Extremely small iron oxide nanoparticles (ESIONs) (Figure S1 in the Supporting Information [SI]) of 3 nm diameter were recently developed as a T_1 MRI contrast agent.[33] These ESIONs were used as hydrophobic building blocks for self-assembly. pH sensitivity was achieved via chemically defined ligand engineering by incorporating ionizable moieties on the polymeric ligand, (see SI, Scheme S1 for experimental details and Figures S2−6, Table S1 in SI for characterization) and chlorin e6 (Ce6) was employed as a photosensitizer for photodynamic therapy (PDT).

Synthesis of ligands and ESIONs. Ligands A and B were synthesized by derivatizing poly(ethylene glycol)−poly(β-benzyl-L-aspartate) (PEG−PBLA) (Scheme S1 in SI) with 1-(3-aminopropyl) imidazole (API) and dopamine (ligand A) or API and 3-phenyl-1-propylamine (PPA) (ligand B). ^{1}H NMR study was performed in National Center for inter-University Research Facilities. ESIONs were synthesized by thermal decomposition of an iron−oleate complex in the presence of oleyl alcohol using a reported procedure.[33] More detailed procedures and material characterizations are described in the SI.

Fabrication of pH-Sensitive Magnetic Nanogrenades (PMNs), Self-Assembled Ligands, and pH-Insensitive Nanoparticle Assemblies (InS-NPs). The assembly was triggered by the dual solvent-exchange method. Briefly, a water-miscible solvent (DMSO) containing the amphiphilic ionic ligands was slowly added to a $CHCl_3$ solution containing the ESIONs followed by evaporation of $CHCl_3$ at 60 °C under vacuum. The DMSO was then dialyzed against water. The ESION-polymer coassembly was induced by solvent exchange from $CHCl_3$ to the more polar DMSO, and solidification was achieved in water which is a poor solvent for both ESIONs and the hydrophobic blocks of the polymer. This facilitated the self-assembly of the core−shell micellar structures in water. The self-assembled ligands were formed using the same process without adding ESIONs, while InS-NPs were formed by using the same process but with the platform ligand rather than ligands A and B. More detailed procedures and characterizations of materials are described in the SI.

RESULTS AND DISCUSSION

Synthesis and Characterization of pH-Sensitive Magnetic Nanogrenades (PMNs). We synthesized Ce6 grafted poly(ethylene glycol)−poly(β-benzyl-L-aspartate) (PEG-PBLA-Ce6) to provide a platform ligand in which the flanking benzyl ester groups readily react with primary amines via nucleophilic attack. Imidazole (pK_a, ~6.8) was then easily

dx.doi.org/10.1021/ja4108287 | J. Am. Chem. Soc. 2014, 136, 5647−5655

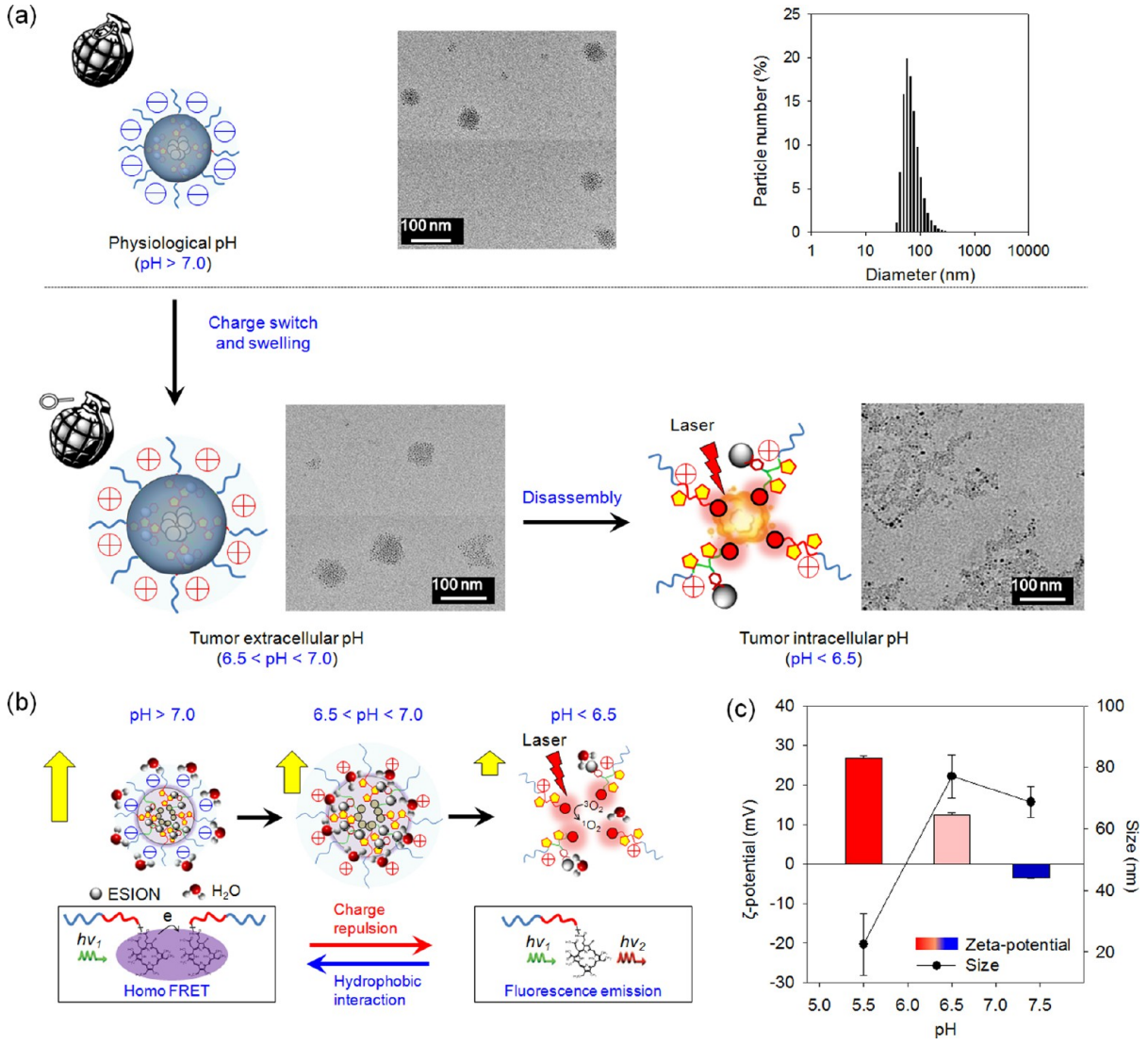

Figure 1. pH-dependent structural transformation and related magnetic/photoactivity change in PMNs. (a) pH-dependent structural transformation behavior in PMNs (inset of (a): TEM images of PMNs at pH 7.4, 6.8, and pH 5.5, DLS measurement of PMN colloidal dispersion at pH 7.4 showing an average diameter of ~70 nm). (b) Schematic representation of pH-dependent structural transformation and related magnetic/photoactivity change in PMNs. (c) Zeta-potential and DLS size measurement of PMNs (0.1 mg/mL) as a function of pH following a 1 h incubation (n = 3). DLS measurements were conducted using a material refractive index of 2.42, solvent refractive index of 1.33 (water) and a viscosity of 0.8872.

incorporated as an ionizable group to impart pH sensitivity to the tumor microenvironment. On the basis of this platform, we further engineered two ligand derivatives: ligands A and B. For ligand A, catechol groups were added to facilitate self-assembly as they can act as high-affinity anchors for iron oxide nanoparticles.[34] In contrast, the hydrophobicity of ligand B was tuned using 3-phenyl-1-propylamine to produce a critical phase transition of PMNs that is activatable by tumor endo/lysosomal pH of ~5.5. The PMNs were fabricated by coassembly of ESIONs, ligand A and ligand B as schematically presented in Scheme 1a. Because ESIONs (~3 nm) were much smaller than the hydrodynamic dimensions of the peptide block of the ligands (~60 residues; length of ~20 nm), the catechol-anchored ligand A could wrap around the periphery of the ESIONs. These functionalized ESIONs can thus be considered polymer−metal analogues of conventional amphiphilic diblock copolymers since the functionalization permitted directed self-assembly of ESIONs into colloidal magneto-core shell structures (Scheme 1b). The hydrophobic core is then composed of the ESIONs and hydrophobic blocks of the tumor-sensing polymeric ligands. Transmission electron microscopy (TEM) (Figure 1a) revealed the particle size of PMNs is ~60 nm. They were well dispersed in water, and the hydrodynamic diameter measured by dynamic light scattering (DLS) was found to be 70 ± 5 nm (Figure 1a and Figure S7 in the SI), which is appropriate for the enhanced permeability and retention (EPR) effect[35] for passive tumor targeting. As a control, we fabricated pH-insensitive nanoparticle assemblies (denoted as InS-NPs) by assembling ESIONs and the platform ligand (see SI for experimental details), which were similarly sized to PMNs (Figure S8 in the SI).

Our new ligand design enabled a two-stage pH activation leading to surface charge reversal in the tumor periphery for increased cell adsorption and permeation as well as endo/lysosomal pH dependent theranostic activity of PMNs. This pH-dependent structural transformation is schematically

dx.doi.org/10.1021/ja4108287 | J. Am. Chem. Soc. 2014, 136, 5647−5655

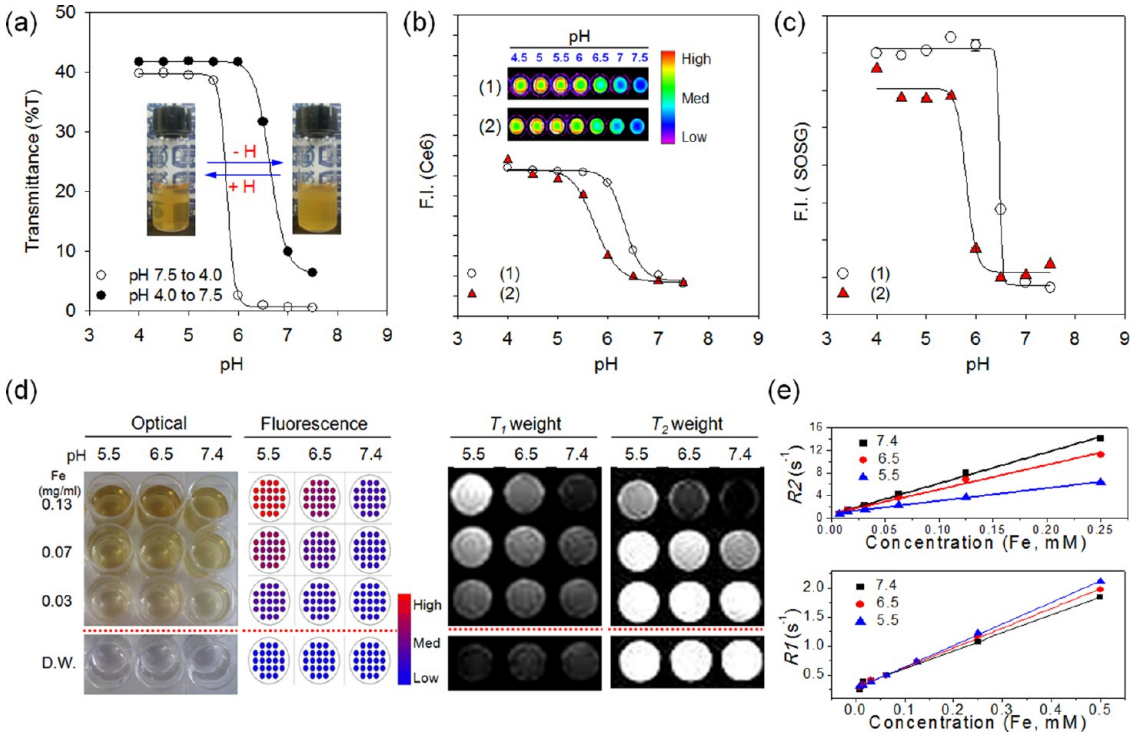

Figure 2. Characterization of the pH-sensitivity of various attributes of PMNs. (a) Transmittance of PMN suspension measured at selected pH values. The inset photo presents data for pH-dependent turbidity of the PMN solution with a transition pH value of ~6.0. The pH was gradually changed from 4.0 to 7.5 (●) and from pH 7.5 to 4.0 (○). (b) pH-dependent fluorescence intensity and near-infrared fluorescence imaging of (1) self-assembled ligands and (2) PMNs. (c) pH-dependent singlet oxygen generation of (1) self-assembled ligands and (2) PMNs. (d) Optical, fluorescence, and MR phantom images (examined in a clinical 1.5 T MRI scanner) of a concentration gradient of PMNs at three different pH values. (e) pH-dependent magnetic relaxation properties of PMNs. (d, e) The positive T_1 MR contrast property of PMNs is quenched at pH 7.4 and recovered at the low pH of 5.5, indicating their capability for accurate T_1 MR imaging of acidic tumor regions.

presented in Figure 1b. First, PMNs are slightly negatively charged at pH 7.4. The drop in pH within the tumor environment causes increased imidazole ionization which reverses the polarity of the complex causing it to swell (Figure 1c), thereby enhancing their payload delivery[36] and cell internalization due to electrostatic interactions with the vicinal anionic cells.[37−39] Upon internalization, the particles further ionize as the endosomal pH decreases to 5.5−6.0. Here the hydrophobic interactions of the core of the PMNs weaken, and the ionized unimers repel each other leading to complete dissociation as confirmed by both DLS (Figure 1c) and TEM (Figure 1a). Acid−base titration (Figure 2a) demonstrated a sharp drop in transmittance (%T) at the critical pH range of 5.5−6.0. When the pH was increased again, %T recovery was hysteretic, thereby demonstrating a reversible pH-dependent assembly/disassembly process. Consequently, the photoactivity, i.e. singlet oxygen generation (SOG) and fluorescence, of PMNs was quenched at pH 7.4 due to fluorescence resonance energy transfer.[40] At pH < 6, the photoactivity was dramatically recovered upon disassembly, similar to that observed for the other self-assembled polymeric ligands (Figure 2b,c). Interestingly, PMNs showed a 2-fold lower critical aggregation concentration (~0.01 mg/mL) than the self-assembled polymeric ligands possibly due to polymer chain entanglement[11,41] indicating their improved colloidal stability (Figure S9 in the SI).

The X-ray diffraction (XRD) pattern of PMNs was similar to that of ESIONs (Figure S10 in the SI), and the PMNs show a weak magnetization because of the spin-canting effect[33] (Figure S11 in the SI). The pH-dependent structural transformation of PMNs in water is expected to affect proton relaxation. Considering the large number of high-spin Fe(III) ions with five unpaired electrons (S = 5/2) on the surface of ESIONs, direct water coordination with Fe^{3+} species is a major contributor to the longitudinal relaxivity ($r1$) of PMNs.[33] The intensity variation of the T_1 MR phantom of PMNs at different pH values (same Fe concentration) was well matched with the corresponding fluorescent imaging results (Figure 2d). PMNs showed an $r1$ of 3.30 $mM^{-1}{\cdot}s^{-1}$ with a transverse relaxivity ($r2$) of 43.95 $mM^{-1}{\cdot}s^{-1}$ at pH 7.4, and a concomitant $r1$-increase and $r2$-decrease was observed as the pH decreased from 7.4 to 5.5 (Figure 2e). It is assumed as pH decreases, ligands become protonated and gain hydrophilicity. Consequently, both the number of coordinated water molecules and the duration of their coordination with Fe^{3+} will increase. Moreover, as pH-induced disassembly occurs, separated ESIONs exhibit a lower $r2$ compared to initial PMNs.[42] Although the efficiency of the contrast effect is evaluated in terms of relaxivity ($r1$), the $r2/r1$ ratio also plays an important role in positive T_1 imaging as an excessively high $r2$ may preclude their use as T_1 contrast agents.[42] As the pH decreases, the $r2/r1$ ratio of PMNs significantly decreases along with $r2$. Finally, the PMNs have a specific $r1$ value of 3.87 $mM^{-1}{\cdot}s^{-1}$ and a low $r2/r1$ ratio of 5.8 at pH 5.5, which results in a bright signal in T_1-weighted imaging. Therefore, the positive T_1 MR contrast of PMNs was quenched at pH 7.4 but greatly recovered at pH 5.5, which indicates PMNs can be used for sensitive T_1 MR imaging of acidic tumor regions. In contrast, MR contrast of InS-NPs was not dependent on pH (Figure S12 in the SI). To the best of our knowledge, this is the first

dx.doi.org/10.1021/ja4108287 | J. Am. Chem. Soc. 2014, 136, 5647−5655

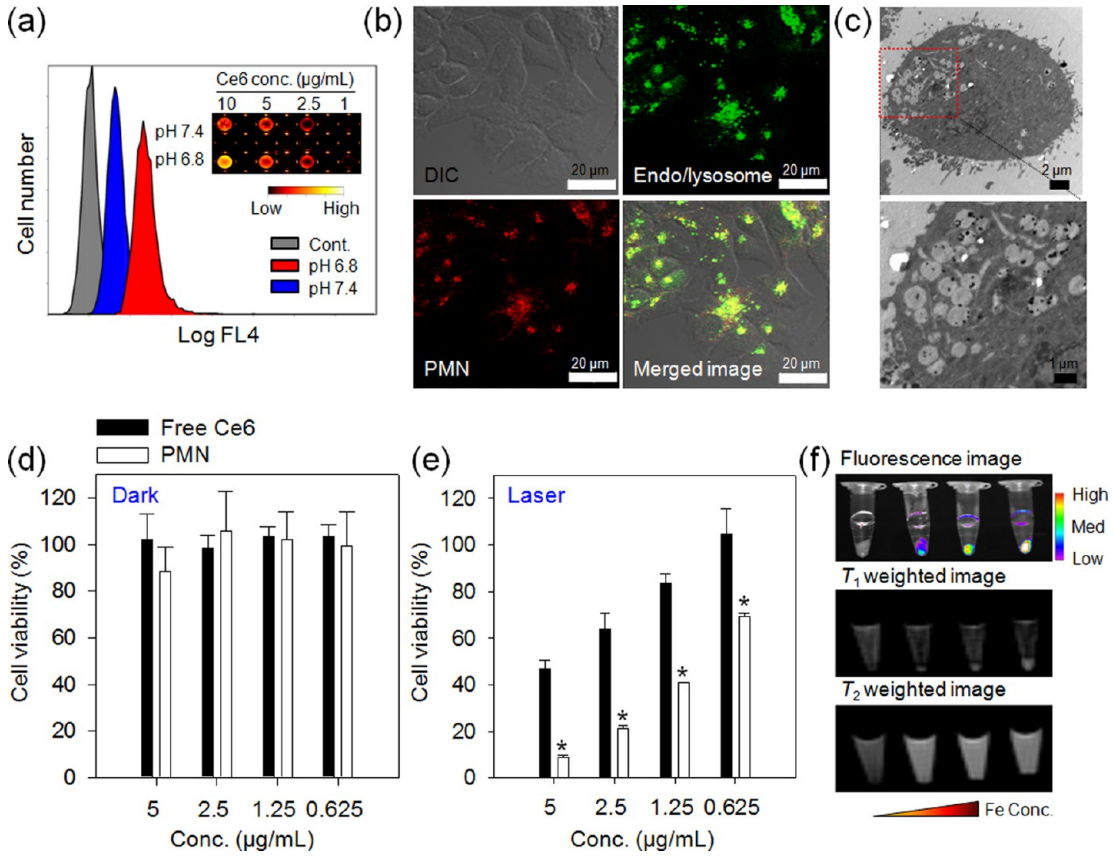

Figure 3. pH-Dependent PMN−cell interaction. (a) Cellular uptake of PMNs (equivalent to 1 μg/mL Ce6) for HCT116 cancer cells at pH 7.4 or 6.8 (4 h incubation) analyzed using flow cytometry. The inset shows near-infrared fluorescence imaging of HCT116 cancer cells treated with different concentrations of PMNs at pH 7.4 and 6.8 (4 h incubation). (b) Confocal microscopy images of activated PMNs in HCT116 cancer cells. The endosomes/lysosomes were stained with Lysotracker Green which selectively labels lysosomes. Scale bar: 20 μm. (c) BioTEM images of PMN uptake by HCT116 cancer cells. (d, e) MTT assays of HCT116 cells exposed to PMNs and free Ce6 (d) without or (e) with laser irradiation. (f) Fluorescence (upper) and MR (lower) images of HCT116 cancer cell pellets (1×10^6 cells) incubated with various concentrations of PMNs (0, 12.5, 25, or 50 μg Fe/mL) for 4 h.

demonstration of biocompatible iron oxide nanoparticles showing pH-sensitive T_1 contrast that can be used for tumor pH-sensitive T_1 MR imaging. Although Gd^{3+}-based T_1 contrast agent can also be designed to respond to pH stimulus,[43] they generally have short blood half-lives, preventing their accumulation in tumors for high-resolution tumor imaging.[44] Furthermore, Gd^{3+}-based contrast agents can be potentially toxic; severe side effects were observed in patients with renal failure that received gadolinium-containing contrast agents, such that the U.S. FDA recently released a warning regarding Gd^{3+}-based MR contrast agents and nephrogenic system fibrosis (NSF).[45,46] While such side effects are quite rare, occurring in less than 5% of patients,[45] we believe iron oxide nanoparticles may provide a more biologically and metabolically compatible alternative.[17,42] The use of biodegradable polymeric peptides for iron oxide-based PMN fabrication gives the final product a longer blood half-life and a greater biocompatibility for clinical translation.

***In vitro* pH Dependent Cancer Cell Uptake and Cell Imaging.** PMNs showed higher cellular uptake at pH 6.8 than at pH 7.4 as evidenced by both fluorescence and flow cytometry results (Figure 3a). In contrast, the cellular uptake of Ce6 and InS-NPs was not affected by changes in pH (Figure S13 in the SI). For cell uptake, we followed the iron oxide nanoparticles by TEM (Figure 3c) which shows uptake in endosomes. We also followed the Ce6 dye by confocal laser scanning microscopy (CLSM) (Figure 3b) which shows the fluorescence of PMNs merges perfectly with that of Lysotracker Green. The existence of the Ce6 signal suggests PMNs indeed disassembled for fluorescence dequenching here in the endosome. Consequently, PMNs showed no cytotoxicity in the dark (Figure 3d) but induced cell death much more efficiently than Ce6 under illumination (Figure 3e) at pH 6.8. MR contrast and fluorescence of human colorectal carcinoma (HCT116) cells labeled with PMNs (Figure 3f) further confirmed their dual-modal imaging capability.

***In vivo* pH-Sensitive Dual-Modal Imaging of Small Tumor.** We performed *in vivo* early stage tumor diagnosis with PMNs. Without conjugation of any tumor-targeting moiety and in contrast to InS-NP injection, PMN injection resulted in significant T_1 enhancement of ultrasmall HCT116 tumors of ~3 mm in diameter (Figure 4a-c), thus confirming their successful tumor targeting and pH-dependent T_1MR contrast effect. Pharmacokinetic studies showed both PMNs ($t_{1/2,\mathrm{PMN}}$ = 2.90 h) and InS-NPs ($t_{1/2,\mathrm{InS\text{-}NP}}$ = 2.19 h) had long blood circulation times (Figure 4d). However, notably, PMN accumulation in tumors was >2-fold higher than that of InS-NPs (Figure 4e and Figure S14 in the SI). Moreover, PMNs also enabled high-resolution fluorescent imaging of tumors in mice (Figures 4f and S15 in SI). Macroscopic fluorescent imaging of excised organs demonstrated significant tumor accumulation of PMNs (Figure S16 in the SI), and subcellular

dx.doi.org/10.1021/ja4108287 | J. Am. Chem. Soc. 2014, 136, 5647−5655

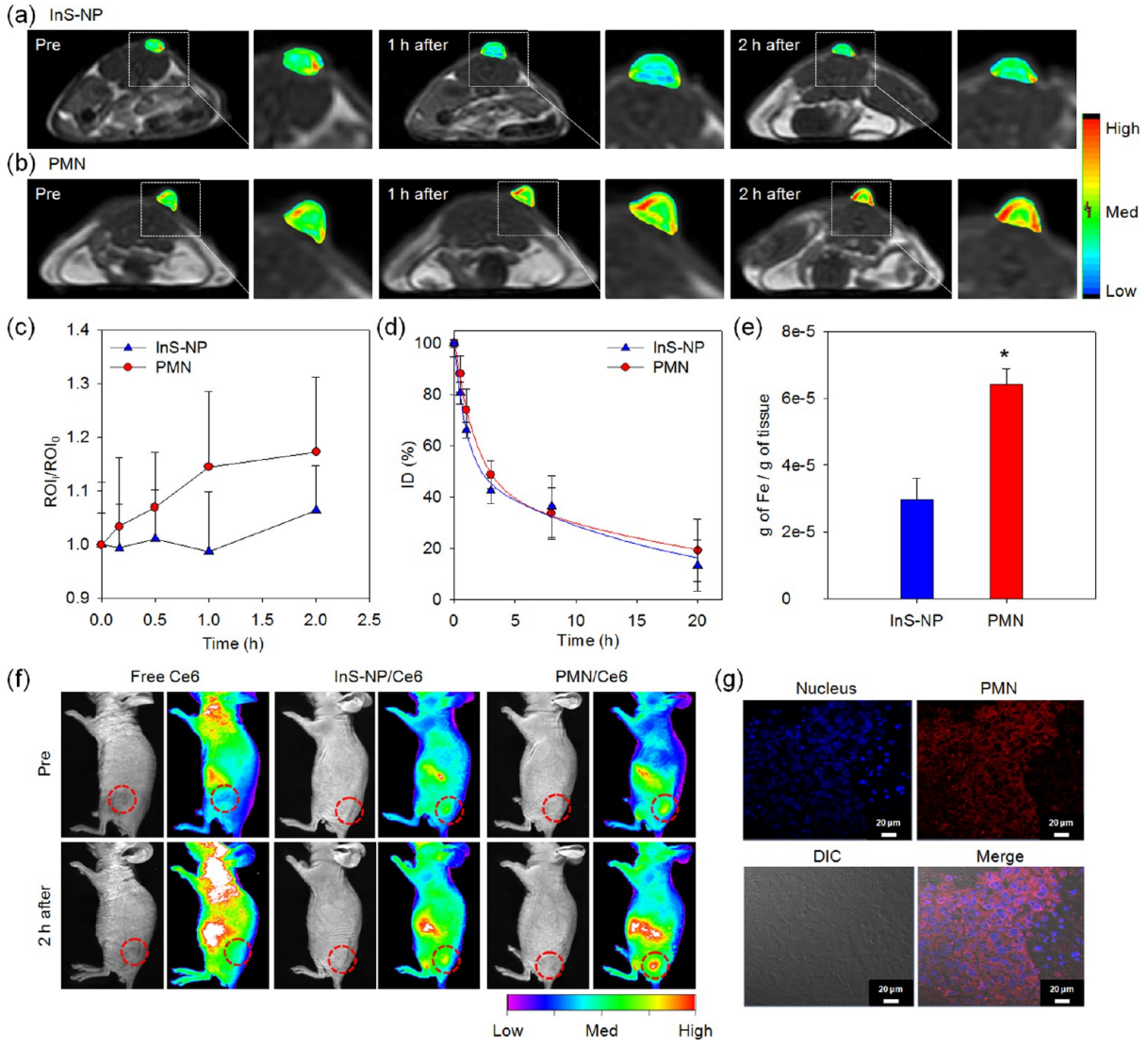

Figure 4. *In vivo* tumor imaging using PMNs. (a, b) *In vivo* T_1-weighted MR images and color-mapped images of tumor sites before and 1 or 2 h after intravenous injection of PMNs or InS-NPs into nude mice bearing HCT116 tumors. Tumors were induced by implanting HCT116 cells subcutaneously in nude mice. After the tumors reached a diameter of 3−5 mm, the tumor-bearing mice were examined in a clinical 1.5 T MRI scanner before and after tail vein injection of PMNs or InS-NPs (2 mg Fe/kg). (c) Plot of signal intensity enhancement (ROI_i/ROI_0) versus time after injection of PMNs and InS-NPs. (d) Blood circulation data (plasma iron concentration vs time) for PMNs and InS-NPs in nude mice (see inset; n = 3 for each group). (e) Inductively coupled plasma atomic emission spectroscopy (ICP-AES) analysis of tumor tissue shows >2-fold increase of PMNs than InS-NPs in HCT116 tumors at 12 h after intravenous injection. Scale bars: 50 μm. (f) *In vivo* NIR imaging of nude mice bearing HCT116 tumors after intravenous injection of PMNs, InS-NPs or free Ce6 (equivalent to 0.2 mg/kg Ce6). (g) CLSM shows Ce6 uptake by tumor cells in tumor tissue of nude mice after intravenous injection of PMNs. Scale bar: 20 μm. The dashed regions in (a, b, f) indicate tumor sites.

CLSM confirmed uptake of PMNs by tumor cells (Figure 4g). These results indicate PMNs are promising candidates for highly efficient early diagnosis of cancer.

Overcome Tumor Heterogeneity and Multidrug Resistance via pH-Responsive PDT. To explore the therapeutic effect of PMNs, *in vivo* photodynamic therapy (PDT) was performed (Figure 5). PDT is a clinically approved, minimally invasive therapeutic procedure for cancer treatment that relies on photosensitizers to produce cytotoxic singlet oxygen generation (SOG) upon irradiation.[47−49] However, currently available photosensitizers lack tumor selectivity which causes undesirable damage to normal tissues. In our PMN system, the activity of the photosensitizer can be self-quenched until it reaches the target tumor site where this suppression can be rapidly reversed by tumor pH stimulus, in particular intracellular pH stimulus, leading to a highly specific region of effect. HCT116 tumor-bearing mice injected with PMNs and then irradiated showed significant tumor regression relative to mice treated with InS-NPs or free Ce6 (Figure 5d,e). In particular, at 1 week postinjection, the tumors were almost completely destroyed with only scar tissue remaining. The enhanced antitumor effect was confirmed by hematoxylin and eosin staining (H&E) and terminal deoxynucleotidyl transferase dUTP nick-end labeling (TUNEL) staining. These results clearly demonstrated that pH-targeted PDT using PMNs was successful in homogeneous HCT116 xenografts.

In order to be a better match to clinical cancer treatment, we further demonstrated the therapeutic effect of PMNs in tumors of more heterogeneous and drug-resistant nature. We hypothesized the pH-targeting approach of PMNs would not

dx.doi.org/10.1021/ja4108287 | J. Am. Chem. Soc. 2014, 136, 5647−5655

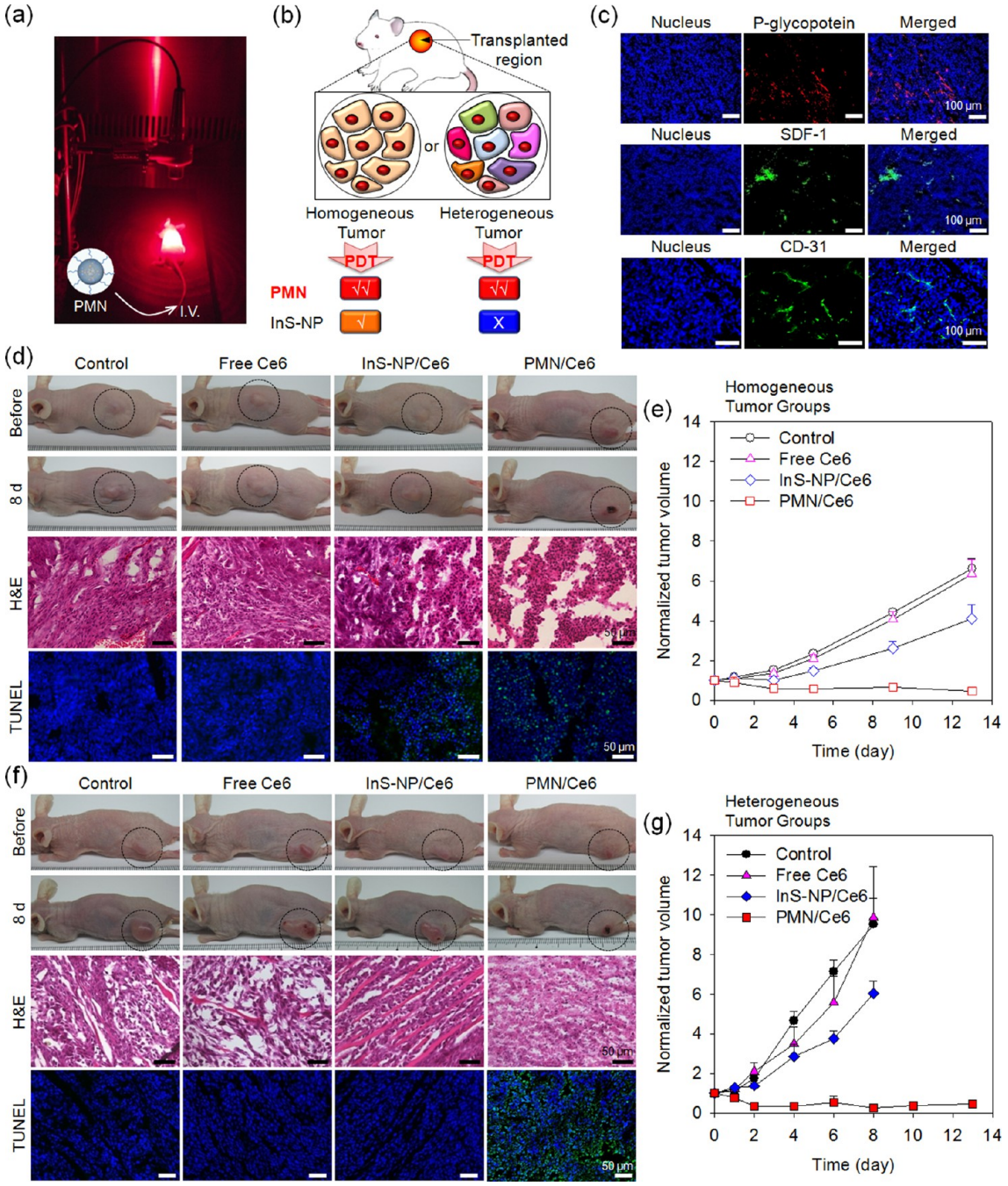

Figure 5. *In vivo* tumor therapy involving PMNs. (a) Photograph showing PMN-based targeted photodynamic therapy (PDT). (b) Schematic illustration and comparison of PDT efficacy of PMNs and InS-NPs in homogeneous and heterogeneous tumors. (c) Immunohistochemical staining of heterogeneous tumors for SDF-1, P-gp and CD31. Scale bar: 100 μm. (d) Upper: Images of mice bearing homogeneous HCT116 tumors before and after PDT activation. Below: Hematoxylin and eosin (H&E) and terminal deoxynucleotidyl transferase dUTP nick-end labeling (TUNEL) staining of tumor tissue sections to determine treatment effectiveness in terms of tumor cell death by apoptosis. For homogeneous HCT116 tumor, most tumor cells were severely destroyed in PMNs treated group, in contrast to control tumor slices collected from InS-NP (some damage) and free Ce6-treated mice (no damage). (e) Homogeneous HCT116 tumor (open dots) volumes in the four treatment groups after treatment. (f) Upper: Images of mice bearing heterogeneous tumors before and after PDT activation. Below: H&E and TUNEL staining of tumor tissue sections to determine treatment effectiveness in terms of tumor cell death by apoptosis. For heterogeneous tumors in the PMN-treated group, many cells in the tumor tissue and microvasculature, as well as fibroblasts, were destroyed, whereas no obvious damage was observed in both InS-NP- and Ce6-treated groups. (g) Heterogeneous tumor (solid dots) volumes in the four treatment groups after treatment. Ten days after inoculating the tumor cells, PDT treatment was performed as follows: group 1, saline only; group 2, free Ce6 only; group 3, InS-NPs; and group 4, PMNs (equivalent to 2 mg/kg body of Ce6). The values are mean ± s.e.m. values (n = 6 mice per group). TUNEL-positive apoptotic cells showed FITC staining within the nucleus or cytoplasm. DAPI counterstaining indicates the nuclear region. Scale bar: 50 μm.

be influenced by tumor heterogeneity, and since PDT kills by a nonspecific mechanism, drug-resistant cells are equally as susceptible as their naïve counterparts. To test this hypothesis, we developed highly heterogeneous and drug-resistant CT26

dx.doi.org/10.1021/ja4108287 | J. Am. Chem. Soc. 2014, 136, 5647−5655

tumors in mice (see Methods in SI for experimental details). The heterogeneous CT26 tumors overexpress P-glycoprotein (P-gp), which is involved in the active efflux of anticancer agents, and stromal cell-derived factor-1 (SDF-1), which induces angiogenesis (CD31) (Figure 5c).[50] Consequently, the CT26 tumors provided a physiologically relevant model of clinical tumors with a much faster growth rate than homogeneous HCT116 tumors. Notably, InS-NPs produced some minor tumor growth inhibition in both the homogeneous HCT116 and heterogeneous CT26 tumors (Figure 5f,g) compared to the untreated control. However, the heterogeneous model grows much more aggressively such that the positive effects observed for InS-NPs are still far too weak. In contrast, PMNs provided the same dramatic tumor destruction in both CT26-tumor-bearing mice and homogeneous HCT116-tumor-bearing mice (Figure 5f,g). In the PMN-treated group, many cells in the tumor tissue and microvasculature as well as fibroblasts showed considerable destruction, whereas no obvious damage was observed in groups treated with InS-NPs or Ce6 (Figure 5f,g). Therefore, pH targeting appears to play an important role in the improved anticancer therapeutic efficacy of PMNs. Consequently, for the first time, we successfully demonstrated treatment of drug-resistant heterogeneous tumor via pH-sensitive PDT, indicating PMNs can be applicable to various tumor treatments including highly drug-resistant heterogeneous tumors. Furthermore, no significant loss in body weight was observed throughout the PDT treatment (Figure S17 in the SI), and a series of *in vivo* biocompatibility tests including a histopathology examination and serum chemistry test (Figure S18 in the SI) demonstrated PMNs are highly biocompatible.

CONCLUSIONS

We demonstrated a new class of anticancer agent, the PMNs, which introduces a self-assembled nanostructure that responds to tumor acidic stimulus. On the basis of such pH-dependent assembly/disassembly, MR imaging and the photoactivity of PMNs can be enhanced when present in the tumor pH environment. The unique pH-responsive mechanism of this particle overcomes two major barriers in cancer therapy: very early-stage diagnosis and treatment of heterogeneous, drug-resistant tumors. The MRI and fluorescence imaging of the PMNs enable dual-modal small tumor diagnosis with a positive imaging result at a tumor diameter of only 3 mm. Furthermore, the enhanced photoactivation of the PMNs within the endosomes of the tumor parenchyma provided superior therapeutic efficacy in both human colorectal carcinoma xenografts and in highly heterogeneous drug-resistant tumors. The combination of favorable pH-sensitive T_1 MR imaging of tumors as well as PDT efficiency allows simultaneous tumor diagnosis and therapy for personalized cancer treatment. The collective results from these studies strongly support the possibility of tumor pH recognizable treatment strategy using PMNs. Overall, the PMN-based tumor pH recognizable treatment strategy may hopefully advance cancer nanotechnology and prove highly valuable for clinical applications.

ASSOCIATED CONTENT

Supporting Information

Detailed experimental procedures for the synthesis and characterizations of PMNs, cell MR imaging, pharmacokinetic analysis, immunohistochemistry, tumor histology, *in vivo* toxicity evaluation of PMNs, *in vitro* and *in vivo* MRI, and *in vitro* and *in vivo* PDT. This material is available free of charge via the Internet at http://pubs.acs.org.

AUTHOR INFORMATION

Corresponding Authors

kna6997@catholic.ac.kr (K.N.)
thyeon@snu.ac.kr (T.H.)

Author Contributions

[#]D.L. and W.P. contributed equally to this work.

Notes

The authors declare no competing financial interest.

ACKNOWLEDGMENTS

T.H. acknowledges financial support by the Research Center Program of Institute for Basic Science (IBS) in Korea. K.N. acknowledges the financial support of the Korea Ministry of Education, Science and Technology through Strategic Research (2011-0028726).

REFERENCES

(1) Kreso, A.; O'Brien, C. A.; van Galen, P.; Gan, O. I.; Notta, F.; Brown, A. M.; Ng, K.; Ma, J.; Wienholds, E.; Dunant, C.; Pollett, A.; Gallinger, S.; McPherson, J.; Mullighan, C. G.; Shibata, D.; Dick, J. E. *Science* **2013**, *339*, 543.

(2) Gerlinger, M.; Rowan, A. J.; Horswell, S.; Larkin, J.; Endesfelder, D.; Gronroos, E.; Martinez, P.; Matthews, N.; Stewart, A.; Tarpey, P.; Varela, I.; Phillimore, B.; Begum, S.; McDonald, N. Q.; Butler, A.; Jones, D.; Raine, K.; Latimer, C.; Santos, C. R.; Nohadani, M.; Eklund, A. C.; Spencer-Dene, B.; Clark, G.; Pickering, L.; Stamp, G.; Gore, M.; Szallasi, Z.; Downward, J.; Futreal, P. A.; Swanton, C. *N. Engl. J. Med.* **2012**, *366*, 883.

(3) Nichols, J. W.; Bae, Y. H. *Nano Today* **2012**, *7*, 606.

(4) (a) Netti, P. A.; Berk, D. A.; Swartz, M. A.; Grodzinsky, A. J.; Jain, R. K. *Cancer Res.* **2000**, *60*, 2497. (b) Gottesman, M. M. *Annu. Rev. Med.* **2002**, *53*, 615.

(5) (a) Trédan, O.; Galmarini, C. M.; Patel, K.; Tannock, I. F. *J. Natl. Cancer Inst.* **2007**, *99*, 1441. (b) Yuan, F.; Dellian, M.; Fukumura, D.; Leunig, M.; Berk, D. A.; Torchilin, V. P.; Jain, R. K. *Cancer Res.* **1995**, *55*, 3752. (c) Matsumura, Y.; Maeda, H. *Cancer Res.* **1986**, *46*, 6387. (d) Popović, Z.; Liu, W.; Chauhan, V. P.; Lee, J.; Wong, C.; Greytak, A. B.; Insin, N.; Nocera, D. G.; Fukumura, D.; Jain, R. K.; Bawendi, M. G. *Angew. Chem., Int. Ed.* **2010**, *49*, 8649.

(6) (a) Horcajada, P.; Chalati, T.; Serre, C.; Gillet, B.; Sebrie, C.; Baati, T.; Eubank, J. F.; Heurtaux, D.; Clayette, P.; Kreuz, C.; Chang, J. S.; Hwang, Y. K.; Marsaud, V.; Bories, P. N.; Cynober, L.; Gil, S.; Férey, G.; Couvreur, P.; Gref, R. *Nat. Mater.* **2009**, *9*, 172. (b) Lee, J. H.; Chen, K. J.; Noh, S. H.; Garcia, M. A.; Wang, H.; Lin, W. Y.; Jeong, H.; Kong, B. J.; Stout, D. B.; Cheon, J.; Tseng, H. R. *Angew. Chem., Int. Ed.* **2013**, *52*, 4384. (c) Zhang, F.; Braun, G. B.; Pallaoro, A.; Zhang, Y.; Shi, Y.; Cui, D.; Moskovits, M.; Zhao, D.; Stucky, G. D. *Nano Lett.* **2012**, *12*, 61. (d) Zhu, X.; Zhou, J.; Chen, M.; Shi, M.; Feng, W.; Li, F. *Biomaterials* **2012**, *33*, 4618. (e) Cheng, Y.; Meyers, J. D.; Broome, A.-M.; Kenney, M. E.; Basilion, J. P.; Burda, C. *J. Am. Chem. Soc.* **2011**, *133*, 2583.

(7) (a) Perrault, S. D.; Chan, W. C. W. *Proc. Natl. Acad. Sci. U.S.A.* **2010**, *107*, 11194. (b) Wang, C.; Cheng, L.; Liu, Y.; Wang, X.; Ma, X.; Deng, Z.; Li, Y.; Liu, Z. *Adv. Funct. Mater.* **2013**, *23*, 3077. (c) Huang, X.; Huang, G.; Zhang, S.; Sagiyama, K.; Togao, O.; Ma, X.; Wang, Y.; Li, Y.; Soesbe, T. C.; Sumer, B. D.; Takahashi, M.; Sherry, A. D.; Gao, J. *Angew. Chem., Int. Ed.* **2013**, *52*, 8074. (d) Chen, Y.; Chen, H.; Shi, J. *Adv. Mater.* **2013**, *25*, 3144. (e) Fan, W.; Shen, B.; Bu, W.; Chen, F.; Zhao, K.; Zhang, S.; Zhou, L.; Peng, W.; Xiao, Q.; Xing, H.; Liu, J.; Ni, D.; He, Q.; Shi, J. *J. Am. Chem. Soc.* **2013**, *135*, 6494.

(8) Piao, Y.; Kim, J.; Na, H. B.; Kim, D.; Baek, J. S.; Ko, M. K.; Lee, J. H.; Shokouhimehr, M.; Hyeon, T. *Nat. Mater.* **2008**, *7*, 242−247.

(9) Zrazhevskiy, P.; Sena, M.; Gao, X. *Chem. Soc. Rev.* **2010**, *39*, 4326.

(10) (a) Bertin, P. A.; Gibbs, J. M.; Shen, C. K.-F.; Thaxton, C. S.; Russin, W. A.; Mirkin, C. A.; Nguyen, S. T. *J. Am. Chem. Soc.* **2006**, *128*, 4168. (b) Lovell, J. F.; Jin, C. S.; Huynh, E.; Jin, H.; Kim, C.; Rubinstein, J. L.; Chan, W. C. W.; Cao, W.; Wang, L. V.; Zheng, G. *Nat. Mater.* **2011**, *10*, 324.
(11) (a) Dhar, S.; Daniel, W. L.; Giljohann, D. A.; Mirkin, C. A.; Lippard, S. *J. Am. Chem. Soc.* **2009**, *131*, 14652. (b) Kim, J.; Lee, J. E.; Lee, S. H.; Yu, J. H.; Lee, J. H.; Park, T. G.; Hyeon, T. *Adv. Mater.* **2008**, *20*, 478.
(12) (a) Cheng, Z.; Al Zaki, A.; Hui, J. Z.; Muzykantov, V. R.; Tsourkas, A. *Science* **2012**, *338*, 903. (b) Kim, C. S.; Tonga, G. Y.; Solfiell, D.; Rotello, V. M. *Adv. Drug. Delivery Rev.* **2013**, *65*, 93.
(13) Xie, J.; Liu, G.; Eden, H. S.; Ai, H.; Chen, X. *Acc. Chem. Res.* **2011**, *44*, 883.
(14) Caldorera-Moore, M. E.; Liechty, W. B.; Peppas, N. A. *Acc. Chem. Res.* **2011**, *44*, 1061.
(15) Lee, D. E.; Koo, H.; Sun, I. C.; Ryu, J. H.; Kim, K.; Kwon, I. C. *Chem. Soc. Rev.* **2012**, *41*, 2656.
(16) Yoo, D.; Lee, J. H.; Shin, T. H.; Cheon, J. *Acc. Chem. Res.* **2011**, *44*, 863.
(17) (a) Smith, B. R.; Zavaleta, C.; Rosenberg, J.; Tong, R.; Ramunas, J.; Liu, Z.; Dai, H.; Gambhir, S. S. *Nano Today* **2013**, *8*, 126. (b) Ling, D.; Hyeon, T. *Small* **2012**, *9*, 1450.
(18) (a) Cole, A. J.; Yang, V. C.; David, A. E. *Trends Biotechnol.* **2011**, *29*, 323. (b) Xu, C.; Sun, S. *Adv. Drug Delivery Rev.* **2013**, *65*, 732. (c) Lu, Z.; Yin, Y. *Chem. Soc. Rev.* **2012**, *41*, 6874.
(19) Kim, J.; Piao, Y.; Hyeon, T. *Chem. Soc. Rev.* **2009**, *38*, 372.
(20) (a) Nie, Z.; Petukhova, A.; Kumacheva, E. *Nat. Nanotechnol.* **2010**, *5*, 15. (b) He, L.; Wang, M.; Ge, J.; Yin, Y. *Acc. Chem. Res.* **2012**, *45*, 1431.
(21) Jin, Y.; Gao, X. *Nat. Nanotechnol.* **2009**, *4*, 571.
(22) Liu, G. L.; Yin, Y.; Kunchakarra, S.; Mukherjee, B.; Gerion, D.; Jett, S. D.; Bear, D. G.; Gray, J. W.; Alivisatos, A. P.; Lee, L. P.; Chen, F. F. *Nat. Nanotechnol.* **2006**, *1*, 47.
(23) Mirkin, C. A.; Letsinger, R. L.; Mucic, R. C.; Storhoff, J. J. *Nature* **1996**, *382*, 607.
(24) Lee, J.; Hernandez, P.; Lee, J.; Govorov, A. O.; Kotov, N. A. *Nat. Mater.* **2007**, *6*, 291.
(25) (a) Lee, H.; Sun, E.; Ham, D.; Weissleder, R. *Nat. Med.* **2008**, *14*, 869. (b) Plush, S. E.; Woods, M.; Zhou, Y.-F.; Kadali, S. B.; Wong, M. S.; Sherry, A. D. *J. Am. Chem. Soc.* **2009**, *131*, 15918.
(26) Rosi, N. L.; Mirkin, C. A. *Chem. Rev.* **2005**, *105*, 1547.
(27) Cao, Y. C.; Jin, R.; Mirkin, C. A. *Science* **2002**, *297*, 1536.
(28) Zagorovsky, K.; Chan, W. C. W. *Angew. Chem., Int. Ed.* **2013**, *52*, 3168.
(29) Taton, T. A.; Mirkin, C. A.; Letsinger, R. L. *Science* **2000**, *289*, 1757.
(30) Pan, Y.; Du, X.; Zhao, F.; Xu, B. *Chem. Soc. Rev.* **2012**, *41*, 2912.
(31) Gallagher, F. A.; Kettunen, M. I.; Day, S. E.; Hu, D.-E.; Ardenkjær-Larsen, J. H.; Zandt, R. i.; Jensen, P. R.; Karlsson, M.; Golman, K.; Lerche, M. H.; Brindle, K. M. *Nature* **2008**, *453*, 940.
(32) (a) Urano, Y.; Asanuma, D.; Hama, Y.; Koyama, Y.; Barrett, T.; Kamiya, M.; Nagano, T.; Watanabe, T.; Hasegawa, A.; Choyke, P. L.; Kobayashi, H. *Nat. Med.* **2008**, *15*, 104. (b) Lee, E. S.; Kim, D.; Youn, Y. S.; Oh, K. T.; Bae, Y. H. *Angew. Chem., Int. Ed.* **2008**, *47*, 2418.
(33) Kim, B. H.; Lee, N.; Kim, H.; An, K.; Park, Y. I.; Choi, Y.; Shin, K.; Lee, Y.; Kwon, S. G.; Na, H. B.; Park, J. G.; Ahn, T. Y.; Kim, Y. W.; Moon, W. K.; Choi, S. H.; Hyeon, T. *J. Am. Chem. Soc.* **2011**, *133*, 12624.
(34) Ling, D.; Park, W.; Park, Y. I.; Lee, N.; Li, F.; Song, C.; Yang, S. G.; Choi, S. H.; Na, K.; Hyeon, T. *Angew. Chem., Int. Ed.* **2011**, *50*, 11360.
(35) (a) Cabral, H.; Matsumoto, Y.; Mizuno, K.; Chen, Q.; Murakami, M.; Kimura, M.; Terada, Y.; Kano, M.; Miyazono, K.; Uesaka, M.; Nishiyama, N.; Kataoka, K. *Nat. Nanotechnol.* **2011**, *6*, 815. (b) Roberts, W. G.; Palade, G. E. *Cancer Res.* **1997**, *57*, 765.
(36) Kim, B.; Han, G.; Toley, B. J.; Kim, C.-k.; Rotello, V. M.; Forbes, N. S. *Nat. Nanotechnol.* **2010**, *5*, 465.
(37) (a) Du, J.-Z.; Du, X.-J.; Mao, C.-Q.; Wang, J. *J. Am. Chem. Soc.* **2011**, *133*, 17560. (b) Yuan, Y. Y.; Mao, C. Q.; Du, X. J.; Du, J. Z.; Wang, F.; Wang, J. *Adv. Mater.* **2012**, *24*, 5476.
(38) Jiang, W.; Kim, B. Y.; Rutka, J. T.; Chan, W. C. W. *Nat. Nanotechnol.* **2008**, *3*, 145.
(39) (a) Gratton, S. E.; Ropp, P. A.; Pohlhaus, P. D.; Luft, J. C.; Madden, V. J.; Napier, M. E.; DeSimone, J. M. *Proc. Natl. Acad. Sci. U.S.A* **2008**, *105*, 11613. (b) Mok, H.; Park, J. W.; Park, T. G. *Bioconjug. Chem.* **2008**, *19*, 797. (c) Lee, E. S.; Na, K.; Bae, Y. H. *Nano Lett.* **2005**, *5*, 325.
(40) (a) Zhang, X.; Rehm, S.; Safont-Sempere, M. M.; Würthner, F. *Nat. Chem.* **2009**, *1*, 623. (b) Zhou, K.; Wang, Y.; Huang, X.; Luby–Phelps, K.; Sumer, B. D.; Gao, J. *Angew. Chem., Int. Ed.* **2011**, *50*, 6109. (c) Zhou, K.; Liu, H.; Zhang, S.; Huang, X.; Wang, Y.; Huang, G.; Sumer, B. D.; Gao, J. *J. Am. Chem. Soc.* **2012**, *134*, 7803.
(41) Nasongkla, N.; Bey, E.; Ren, J.; Ai, H.; Khemtong, C.; Guthi, J. S.; Chin, S.-F.; Sherry, A. D.; Boothman, D. A.; Gao, J. *Nano Lett.* **2006**, *6*, 2427.
(42) Lee, N.; Hyeon, T. *Chem. Soc. Rev.* **2012**, *41*, 2575.
(43) (a) Zhang, S.; Wu, K.; Sherry, A. D. *Angew. Chem., Int. Ed.* **1999**, *38*, 3192. (b) Aime, S.; Barge, A.; Delli Castelli, D.; Fedeli, F.; Mortillaro, A.; Nielsen, F. U.; Terreno, E. *Magn. Reson. Med.* **2002**, *47*, 639. (c) Garcia–Martin, M. L.; Martinez, G. V.; Raghunand, N.; Sherry, A. D.; Zhang, S.; Gillies, R. J. *Magn. Reson. Med.* **2006**, *55*, 309.
(44) L. Villaraza, A. J.; Bumb, A.; Brechbiel, M. W. *Chem. Rev.* **2010**, *110*, 2921.
(45) Penfield, J. G.; Reilly, R. F. *Nat. Clin. Pract. Nephrol.* **2007**, *3*, 654.
(46) Sieber, M. A.; Pietsch, H.; Walter, J.; Haider, W.; Frenzel, T.; Weinmann, H.-J. *Invest. Radiol.* **2008**, *43*, 65.
(47) (a) Dolmans, D. E.; Fukumura, D.; Jain, R. K. *Nat. Rev. Cancer* **2003**, *3*, 380. (b) Master, A.; Livingston, M.; Sen Gupta, A. *J. Controlled Release* **2013**, *168*, 88.
(48) (a) Ling, D.; Bae, B. C.; Park, W.; Na, K. *Biomaterials* **2012**, *33*, 5478. (b) Vaidya, A.; Sun, Y.; Ke, T.; Jeong, E. K.; Lu, Z. R. *Magn. Reson. Med.* **2006**, *56*, 761. (c) Vaidya, A.; Sun, Y.; Feng, Y.; Emerson, L.; Jeong, E. K.; Lu, Z. R. *Pharm. Res.* **2008**, *25*, 2002.
(49) Agostinis, P.; Berg, K.; Cengel, K. A.; Foster, T. H.; Girotti, A. W.; Gollnick, S. O.; Hahn, S. M.; Hamblin, M. R.; Juzeniene, A.; Kessel, D.; Korbelik, M.; Moan, J.; Mroz, P.; Nowis, D.; Piette, J.; Wilson, B. C.; Golab, J. *CA Cancer J. Clin.* **2011**, *61*, 250.
(50) Orimo, A.; Gupta, P. B.; Sgroi, D. C.; Arenzana-Seisdedos, F.; Delaunay, T.; Naeem, R.; Carey, V. J.; Richardson, A. L.; Weinberg, R. A. *Cell* **2005**, *121*, 335.